OPEN ACCESS
IOP Publishing
Measurement Science and Technology
Meas. Sci. Technol. **28** (2017) 012003 (19pp)
doi:10.1088/1361-6501/28/1/012003

Topical Review

Wide-field TCSPC: methods and applications

Liisa M Hirvonen and Klaus Suhling

Department of Physics, King's College London, Strand, London WC2R 2LS, UK

E-mail: klaus.suhling@kcl.ac.uk

Received 16 September 2015, revised 5 October 2016
Accepted for publication 12 October 2016
Published 1 December 2016

Abstract

Time-correlated single photon counting (TCSPC) is a widely used, robust and mature technique to measure the photon arrival time in applications such as fluorescence spectroscopy and microscopy, LIDAR and optical tomography. In the past few years there have been significant developments with wide-field TCSPC detectors, which can record the position as well as the arrival time of the photon simultaneously. In this review, we summarise different approaches used in wide-field TCSPC detection, and discuss their merits for different applications, with emphasis on fluorescence lifetime imaging.

Keywords: time-correlated single photon counting, fluorescence lifetime imaging, microchannel plate, single-photon avalanche diode array, single photon detection

(Some figures may appear in colour only in the online journal)

List of acronyms

APD	Avalanche photodiode
ASIC	Application specific integrated circuit
CCD	Charge-coupled device
CMOS	Complementary metal oxide semiconductor
EB	Electron-bombarded
FLIM	Fluorescence lifetime imaging
FRET	Förster resonance energy transfer
IRF	Instrument response function
KID	Kinetic induction detector
LIDAR	Light detection and ranging
MCP	Microchannel plate
PLIM	Phosphorescence lifetime imaging
PMT	Photomultiplier tube
SAF	Supercritical angle fluorescence
SNSPD	Superconducting nanowire single-photon detector
SPAD	Single-photon avalanche diode
SPIM	Selective/single plane illumination microscopy
STJ	Superconducting tunnel junction
TAC	Time-to-amplitude converter
TCSPC	Time-correlated single photon counting
TDC	Time-to-digital converter
TES	Transition edge sensor
TIRF	Total internal reflection fluorescence

1. Introduction

1.1. The photon

In 1900, the German theoretical physicist Max Planck devised a theoretical model to explain the blackbody spectrum, experimental data for which had been well known for many years. Planck considered hypothetical material oscillators that can only emit and absorb electromagnetic radiation in discrete, quantized form and not in continuously varying quantities, especially not in arbitrarily small amounts. Although he did not explicitly propose that light is quantized, he postulated that the energy ϵ of these material oscillators is proportional to their oscillation frequency ν

$$\epsilon = h\nu \quad (1)$$

where h is now known as Planck's constant. Five years later, Albert Einstein used this concept to explain the photoelectric effect, for which experimental data had also been available for many years but defied explanation on the basis of the wave theory of light. Einstein proposed a model whereby light was emitted, absorbed, and propagated in free space in quantized form [1], and introduced the smallest unit of energy of electromagnetic radiation. He called these units *Lichtquant* (quantum of light), and the word 'photon' was introduced in 1926 by the chemist Gilbert Lewis [2]. Einstein also used the photon to explain absorption and emission of radiation, including stimulated emission—the key concept for the laser. In particle physics, the photon is an integer spin particle, a boson, with spin 1. A photon is a 'quantized field', it always travels at the speed of light and has a momentum, but no mass, and no charge [3]. It does not decay[1].

1.2. Experimental detection of photons

Experimental efforts to detect photons were based on two separate discoveries. The photoelectric effect was first observed by Heinrich Hertz in 1887 [4], and in 1905 Einstein established that it was a quantum mechanical effect, where individual photons transfer their energy to single electrons [1]. The photoelectric effect provides means to convert single photons into an electronic signal. However, the electronic signal of one electron is too small to be detected. This problem was overcome by the secondary emission principle, which was discovered in 1902 by Louis Austin and H Starke [5]. It allows electron multiplication and hence gain to be introduced, so that the signal can be amplified and measured.

First reports on phototubes appeared in the 1920s and 1930s, in a race to develop television camera technology. The first demonstrations of working photomultiplier tubes (PMTs) were documented in mid-1930s [6–8], and these devices were shown to be single photon sensitive only a few years later [9]. PMTs found many applications in physics research (early applications include scintillation counters) and are still widely used today. They consist of a photocathode, up to a dozen discrete dynodes, each at a higher potential than the previous one, and an anode, all in vacuum [10].

1.3. Time-correlated single photon counting

The origin of time-correlated single photon counting (TCSPC) lies in particle physics. In 1929, Walther Bothe and Werner Kohlhörster published a method to measure the coincidence of penetrating charged particles in cosmic rays [11]. Inspired by their paper, in 1930 Bruno Rossi invented the first practical electronic coincidence circuit [12] which was rapidly adopted in experiments all around the world, and also became a precursor of the AND logic circuits of electronic computers. By the addition of a delay, this coincidence method evolved to measure delayed coincidence, and thus provided the means for time-resolved measurements. In 1942, Rossi published a method to measure the amplitude of the signal as a function of the delay between pulses—an invention he referred to as the 'time circuit', and is nowadays know as the time-to-amplitude converter (TAC) [13].

A TAC typically charges a capacitor upon receipt of a 'start' pulse, and stops charging it when a 'stop' pulse arrives, such that the capacitor charge is proportional to the time elapsed between 'start' and 'stop'. This charge is converted to a voltage output proportional to the time difference between two pulses (start and stop). Rossi used this for measuring the disintegration curve of mesotrons at rest ($\tau = 2.3 \pm 0.2\ \mu$s), and it became a popular method to measure short radioactive decay times, with time resolution improved to $\sim 8 \times 10^{-11}$ s in the 1950s [14].

In the 1960s photon counting was used in photon correlation spectroscopy which allowed the measurement of diffusion coefficients—a technique that became dynamic light scattering [15]. In 1961, Lowell Bollinger and George Thomas generalised the scintillation measurements to include any type of radiation [16], and flashlamps with optical pulse widths of around ~2 ns became available in 1960s, enabling TCSPC: This is essentially a delayed coincidence method, whereby the arrival time of a single photon is measured relative to an excitation pulse. The accumulation of many single photons then represents the intensity decay of the sample, as long as no photons are lost due to pile-up, and the linearity between intensity and collected photons holds.

The first reports that use TCSPC in the measurement of fluorescence decays appear in the early 1970s [17–19], and TCSPC was soon widely used for time-resolved spectroscopy, and in particular the measurement of fluorescence lifetimes in solutions. Flashlamps used kHz repetition rates [20], but lasers, with picosecond excitation pulses at MHz repetition rates, sped up the measurements significantly and advanced this field enormously [21].

The development of laser scanning confocal microscopes enabled TCSPC-based fluorescence lifetime imaging (FLIM). This method was developed in the late 1980s [22] and early 1990s before being more widely applied in the late 1990s [23].

Single photon detection techniques and applications have been reviewed recently by Buller & Collins [24], Hadfield [25], and Eisaman *et al* [26].

1.4. Wide-field TCSPC

In conventional TCSPC spectroscopy, single point detectors are typically used to collect a fluorescence decay curve [27]. In scanning-based TCSPC FLIM, the image is created by raster scanning the sample and collecting fluorescence decays in each pixel of the image one after another, also using single point detectors [22, 23]. To perform wide-field TCSPC imaging, a position-sensitive detector is required, effectively a single photon sensitive camera which can detect the position and arrival time of individual photons. Such a device, a photon counting image intensifier, has been used in astronomy

[1] The Nature milestone series 'Photons' details background and context of the development of the understanding of light and its basic unit, the photon. www.nature.com/milestones/milephotons/index.html

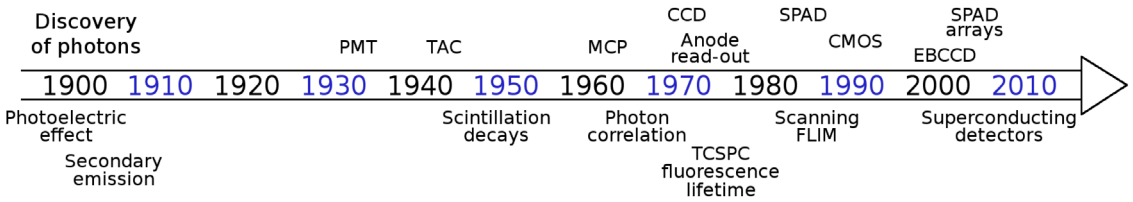

Figure 1. Brief schematic timeline of single photon counting technology. Wide-field single photon counting became possible in the 1970s by the combination of wide-field single photon sensitive detectors with CCD or position-sensitive anode read-out. Although these methods are still in use today and continue to be developed (with CMOS technology replacing CCDs), recent developments in SPAD array and superconducting detector technology are also currently advancing this field at a fast pace.

for low-light level detection. There are various technological implementations of photon counting image intensifiers, e.g. a cascade intensifier [28] was used on the Hubble space telescope's faint object camera [29, 30], but the most modern implementations of this technique employ microchannel plates (MCPs), as discussed below in section 4.1.

With the increasing number of applications of photon counting techniques in different fields of science and technology, from DNA sequencing [31] to interplanetary communications [32], there is a growing need for this technology [24–26, 33]. MCPs are now a mature technology which still continues to be used widely, but in recent years other wide-field photon counting methods have become available that show great promise, including single photon avalanche diode (SPAD) arrays and detectors based on superconducting detector technology. See figure 1 for a timeline of single photon technology. This review gives an overview of the recent developments in the different approaches to wide-field TCSPC, and discusses their merits for different applications in fluorescence lifetime imaging microscopy. Different techniques used for wide-field single photon counting are outlined in section 4, while section 5 discusses the applications of these techniques in the context of fluorescence lifetime imaging microscopy.

2. Theory

2.1. Photon counting

Photon detection follows a Poissonian distribution, which is an approximation of the binomial distribution to describe the probability of 'yes' or 'no' outcomes in trials in the limit where the number of possible outcomes becomes so large that the probability of each outcome is very small and approaches zero [34].

In TCSPC, if the sample emits an average of $\bar{z}$ photons per excitation cycle, according to the Poissonian distribution the probability p_n^{ph} that exactly n photons are emitted after one excitation pulse is

$$p_n^{\mathrm{ph}} = \frac{\bar{z}^n}{n\,!}\mathrm{e}^{-\bar{z}}. \tag{2}$$

How many of these photons are detected depends on the detector quantum efficiency q. This follows a binomial distribution, leading to the probability of detecting k photoelectrons created by the n photons emitted per excitation cycle

$$p_k = \frac{(q\bar{z})^k}{k\,!}\mathrm{e}^{-q\bar{z}}, \tag{3}$$

so the Poissonian statistics are preserved.

Since the sum of all probabilities is one, i.e. $\sum_{k=0}^{\infty} p_k = 1$, the number of detector signals N_D is given by the number of excitation pulses N_{rep} multiplied by the probability of detecting the photons:

$$\begin{aligned} N_D &= N_{\mathrm{rep}}\sum_{k=0}^{\infty} p_k = N_{\mathrm{rep}}\sum_{k=1}^{\infty} p_k = N_{\mathrm{rep}}(1-p_0) \\ &= N_{\mathrm{rep}}(1-\mathrm{e}^{-q\bar{z}}) = N_{\mathrm{rep}}\left(q\bar{z} - \frac{(q\bar{z})^2}{2\,!} + \frac{(q\bar{z})^3}{3\,!} \mp \ldots\right). \end{aligned} \tag{4}$$

The average number of detected photons per excitation pulse, α, can then be obtained from the ratio

$$\alpha = \frac{N_D}{N_{\mathrm{rep}}} = 1 - \mathrm{e}^{-q\bar{z}} = q\bar{z} - \frac{(q\bar{z})^2}{2\,!} + \frac{(q\bar{z})^3}{3\,!} \mp \ldots, \tag{5}$$

i.e. α scales linearly with $q\bar{z}$ only when the probability of detecting multiple events after one excitation pulse is negligible. The error in equation (5) is smaller than the first term which is neglected, and it is negligible if it is smaller than other sources of error, e.g. Poisson noise which is given by the square root of the number of counts [34]. It is important to note that due to Poisson statistics, there is always a chance to detect two photons after one excitation pulse—this probability can never be exactly zero, and it is independent of the time scale used, picoseconds or microseconds, and it is also independent of the technological implementation of TCSPC, using a single TAC, multiple TACs, [35], TDCs [36, 37] or imaging. It is just a question of how much pile-up can be tolerated, for low peak counts more than for very high peak counts [38]. An example of this effect is shown in figure 2 where an increase in α leads to multiple photons in one excitation cycle of which only the first one to arrive is timed and recorded, thus distorting the decay. The Poissonian statistics in photon counting mean that the longer the measurement time, the more counts are accumulated and hence the smaller the uncertainty, as the standard deviation is the square root of the number of counts [34]. The photon counting approach also allows measurements over a large dynamic range.

In addition, TCSPC detector and electronics have a dead-time (time needed for the detector and the electronics

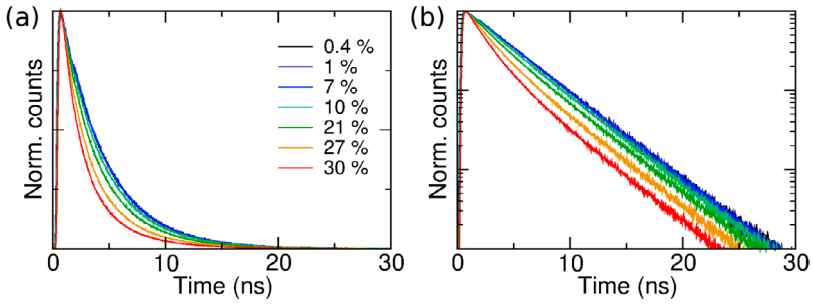

Figure 2. Photon pile-up of a fluorescein decay measured with a point detector; as the count rate increases, the initially monoexponential decay becomes shorter and non-exponential. The photon detection rate is indicated as % of the excitation repetition rate. (a) Linear scale, (b) semilogarithmic scale.

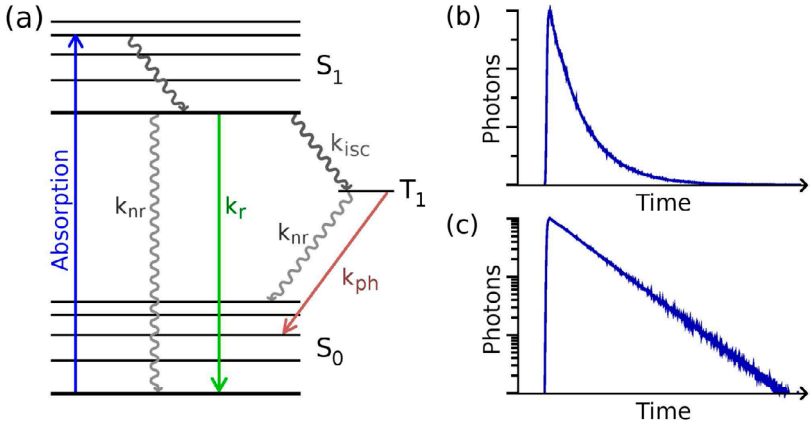

Figure 3. Jablonski energy level diagram showing the transition from ground state S_0 to the first excited state S_1 (absorption) and relaxation via non-radiative transition (k_{nr}) and fluorescence (k_r). The fluorophore can also undergo intersystem crossing to a triplet state T_1 (k_{isc}), from where it can return to the ground state either nonradiatively (k_{nr}) or radiatively (phosphorescence, k_{ph}). (b) A schematic fluorescence decay, where the fluorescence intensity decays over time according to an exponential decay law. (c) A semilogarithmic plot of the same fluorescence decay, which appears as a straight line for a single-exponential decay.

to recover) and, for TAC-based TCSPC implementation, can typically only detect a maximum of one photon per excitation pulse. In practice this means that the count rate cannot exceed the inverse deadtime, and a useful count rate of half the inverse deadtime has been defined [39]. The effect of such a deadtime is typically not the distortion of fluorescence decay curves, but a loss of photons [40].

2.2. Fluorescence

A fluorophore can be sent from the ground state S_0 to the first excited state S_1 by the absorption of a photon (figure 3(a)). The fluorescence lifetime τ is the average time a fluorophore remains in the electronically excited state after excitation before returning to the ground state. τ is defined as the inverse of the sum of the rate parameters for all excited state depopulation processes:

$$\tau = \frac{1}{k_r + k_{nr}} \tag{6}$$

where k_r is the radiative rate constant and k_{nr} the non-radiative rate constant. k_{nr} is the sum of the rate constant for internal conversion, k_{ic}, and the rate constant for intersystem crossing to the triplet state, k_{isc}, so that $k_{nr} = k_{ic} + k_{isc}$.

$\tau_0 = k_r^{-1}$ is the natural or radiative lifetime which is related to the fluorescence lifetime τ via the fluorescence quantum yield ϕ:

$$\phi = \frac{\tau}{\tau_0} = \frac{k_r}{k_r + k_{nr}} = \frac{1}{1 + \frac{k_{nr}}{k_r}} \tag{7}$$

The fluorescence quantum yield can be thought of as the ratio of the number of fluorescence photons emitted to the number of photons absorbed (regardless of their energy) and is usually less than one. And since $\phi\tau_0 = \tau$, τ_0 is the longest lifetime the fluorophore can have, i.e. when it always returns to the ground state through a radiative transition and $k_{nr} = 0$.

After an ensemble of fluorophores is excited, the fluorophores N will return to the ground state according to the rate equation

$$dN = (k_r + k_{nr})N(t)dt \tag{8}$$

where t is the time. This also applies to repeatedly excited single molecules where the fluorescence lifetime represents a measure of the emission probability after a certain time. Integration, and taking into account that the fluorescence intensity $I(t)$ is proportional to the excited state population $N(t)$ yields

$$I(t) = I_0 e^{-\frac{t}{\tau}} \tag{9}$$

where I_0 represents the fluorescence intensity at $t = 0$ and τ is the fluorescence lifetime. The decay of the fluorescence

intensity thus follows an exponential decay law, see figure 3(b) [41]. τ is the time it takes for the fluorescence intensity to decay from its peak value to $e^{-1} \approx 37\%$ of its peak value. Note that on a logarithmic fluorescence intensity scale, a mono-exponential decay conveniently appears as a straight line which allows simple visual inspection of the fluorescence decay behavior (figure 3(c)). If there are many different contributions to the measured lifetime, the measured lifetime is a sum of exponentials:

$$I(t) = A_1 \mathrm{e}^{-\frac{t}{\tau_1}} + A_2 \mathrm{e}^{-\frac{t}{\tau_2}} + \ldots + A_n \mathrm{e}^{-\frac{t}{\tau_n}} \tag{10}$$

where A_n are the amplitudes and τ_n the lifetimes of the contributing components. In practice, the number of exponentials that can be fitted reliably is typically limited to two or three, depending on the number of collected photons [38].

In single-photon lifetime measurements the sample is usually excited with a short pulse of light, $p(t)$. The measured decay I_{meas} is a convolution of the excitation pulse and the fluorescence decay:

$$I_{\mathrm{meas}} = \int_0^t I(t')p(t-t')\mathrm{d}t' = \int_0^t I(t-t')p(t')\mathrm{d}t' = I \otimes p \tag{11}$$

where $\otimes$ is the convolution operator. $p(t)$ is called the instrument response function (IRF), and it is often measured using a sample with much shorter lifetime than the width of the excitation pulse [42], or a scattering solution [27]. The experimentally measured IRF not only takes into account the excitation pulse, but also the response (i.e. timing accuracy) of the instrument used for the measurement. The temporal full width at half maximum (FWHM) of the IRF Δt_{IRF} is given by [43]

$$\Delta t_{\mathrm{IRF}}^2 = \Delta t_{\mathrm{optical}}^2 + \Delta t_{\mathrm{tts}}^2 + \Delta t_{\mathrm{jitter}}^2 \tag{12}$$

where $\Delta t_{\mathrm{optical}}$ is the optical pulse width, Δt_{tts} is the transit time spread of the detector and $\Delta t_{\mathrm{jitter}}$ is the jitter of the electronics. MCP-detectors can achieve transit time spreads of few tens of picoseconds, while mode-locked lasers can deliver femtosecond optical pulses. Under these conditions, IRF widths of $\sim$20 ps are possible. More commonly used diode lasers and LEDs have wider optical pulses, but, in any case, if the IRF is determined experimentally, it can be deconvolved from the decay and the measurement of lifetimes even shorter than the IRF width can be possible.

3. Fluorescence microscopy and fluorescence lifetime imaging (FLIM)

In the life sciences, optical microscopy techniques are powerful tools, because they allow non-destructive and minimally invasive observation of living cells and tissues. Fluorescence microscopy combines single-molecule sensitivity, molecular specificity, sub-cellular resolution and real-time data collection from live cells with negligible cytotoxicity, so that dynamics and function can be observed and quantified [44]. Fluorescence imaging and localization well below the spatial resolution limit given by classical optical diffraction can be achieved with super-resolution techniques—a fast moving and rapidly expanding field, which was honoured with the chemistry Nobel prize 2014 [45]. Detector development is also an important aspect of progress in this field; the charge-coupled device (CCD) camera—the invention of which was rewarded with half of the Nobel prize in physics in 2009 [46, 47]—has played a significant role in advancing fluorescence microscopy.

In addition to localising fluorescent labels, the fluorescence can also provide information about their environment, via their spectral properties, polarization or lifetime. The fluorescence lifetime can be a function of viscosity, temperature, pH, ion or oxygen concentrations, glucose, refractive index or polarity, and of interaction with other molecules, e.g. via Förster resonance energy transfer (FRET) [48–51]. Autofluorescence lifetime measurements can show the metabolic state of cells, and are increasingly used in clinical diagnostics. Fluorescence lifetime measurements, combined with imaging (fluorescence lifetime imaging, FLIM) can map the fluorescence lifetimes in every pixel, where the different lifetimes can be encoded in pseudo-colours, e.g. blue for short lifetimes and red for long lifetimes. The resulting FLIM images show contrast according to the fluorescence lifetime and can therefore be viewed as viscosity maps, ion concentration maps or temperature maps, and they are independent of the fluorophore concentration.

There are different technological implementations of FLIM, and the detector plays an important role in obtaining the picosecond time resolution needed to measure fluorescence decays. TCSPC approaches afford the best signal-to-noise ratio [52–54], an important aspect in view of the limited photon budget emitted by the fluorophores before they are irreversibly bleached [55]. The advantages of TCSPC stem from its the digital nature, based on whether a single photon is detected after an excitation pulse, or not, and include a high dynamic range, high sensitivity, linearity and well-defined Poisson statistics.

TCSPC-based FLIM is straight-forward to implement with confocal or multiphoton excitation beam scanning microscopy. This approach provides intrinsic optical sectioning, and employs single point or single pixel detectors, and the image is created pixel by pixel by raster scanning the focal spot over the sample [56]. However, there are a number of microscopy methods that employ a camera, for example lightsheet, total internal reflection fluorescence (TIRF) and supercritical angle fluorescence (SAF) microscopy, super-resolution fluorescence microscopy methods based on localisation or re-scan confocal and structured illumination microscopy, as well as optical sectioning methods with speckle illumination, spinning disk, temporal focussing or structured illumination. In order to harness the advantages of TCSPC for these microscopy methods, a single photon sensitive camera with picosecond time resolution is required. While microsecond and sub-microsecond time resolution wide-field TCSPC methods based on fast cameras and photon counting image intensifiers have been demonstrated, picosecond time resolution wide-field TCSPC methods are rarely used for FLIM.

There are a number of position-sensitive picosecond resolution read out schemes for intensifiers, either based on charge division techniques or pulse propagation techniques. In addition, the recent development of SPAD array detectors

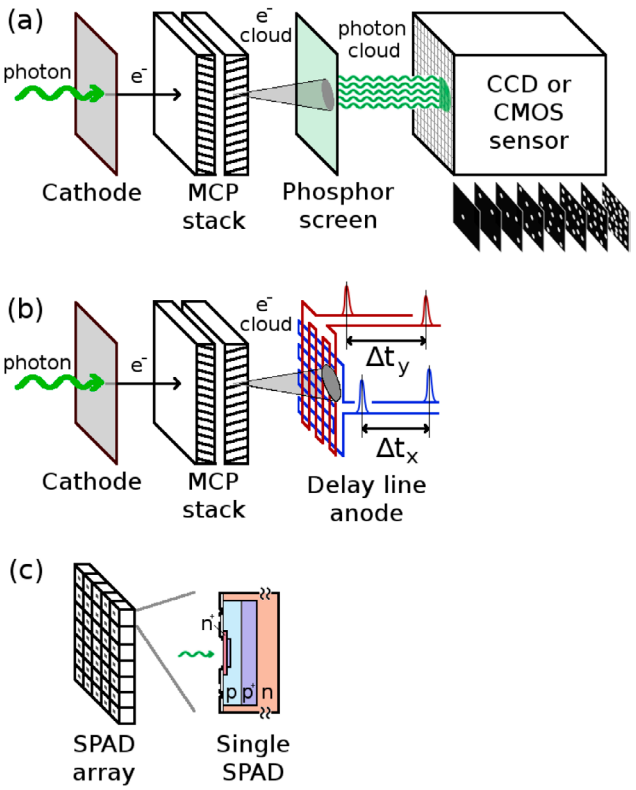

Figure 4. Schematic overview of wide-field TCSPC methods. (a) Camera with MCP image intensifier, (b) MCP detector with a delay line anode, (c) SPAD array.

with picosecond timing capabilities hold great promise for the advancement of time-resolved fluorescence microscopy [57] as discussed below.

4. Wide-field TCSPC methods

Wide-field TCSPC requires the position of the arriving photon to be measured and recorded simultaneously with its arrival time, and it is also known as time and space correlated single photon counting (TSCSPC) [58, 59]. Image intensifier detectors have been used for wide-field single photon detection since the 1960s. Early applications in astronomy did not require the photon arrival time to be measured: the amplified photon events were simply recorded with a camera, and the frames added to form the final image. This method was used, for example, on the Hubble space telescope's faint object camera [29, 30]. The time resolution of such an approach is given by the frame rate of the camera, typically 10s of Hz [60]. With recent developments in CMOS sensor technology, cameras can now reach MHz frame rates, allowing microsecond lifetimes to be measured directly with intensified CMOS cameras (figure 4(a)), as discussed in section 4.1.1. However, for the measurement of nanosecond fluorescence lifetimes, picosecond timing accuracy is essential. The MCPs themselves are capable of timing the photon arrival with a precision of a few tens of picoseconds [10, 39], and the anode can record the position of the photon event. Different read-out architectures have been developed, where the electrons from the MCPs are read out directly with a position-sensitive anode (figure 4(b)), see section 4.1.2. Besides MCP-based detectors, recent advances in SPAD array (figure 4(c), section 4.2) and superconducting detector (section 4.3) technology look very promising to improve and advance wide-field TCSPC.

4.1. Microchannel plates

The concept of an MCP, which consists of continuous dynodes rather than discrete dynodes, as in conventional photomultipliers, was conceived in the 1930s [61], (coincidentally around the same time as PMTs), although the first working devices were not produced until early 1960s [62, 63]. Like PMTs, the operating principle of MCPs is also based on the amplification of electrons via secondary emission, but because an MCP has many separate channels, it can additionally provide spatial resolution. Photon counting imaging where the amplified photon events were imaged with a camera was employed by astronomers due to the exquisite sensitivity this method offered at the time, replacing cascade intensifiers. A decade later, the first position-sensitive read-out anodes were developed [64, 65] which allowed the position of each photon to be correlated with the arrival time provided by the MCP.

A microchannel plate consists of a regular array of tiny tubes (microchannels) where electrons are accelerated from one side of the plate to the other through a high voltage (typically a few kV). The microchannels are usually straight and round with $\sim$10 μm in diameter and a centre-to-centre distance of $\sim$15 μm, although smaller ones, down to 3 μm [66], have been reported [67, 68]. They have traditionally been made by repeatedly pulling glass capillaries until the required diameter is reached, and stacking them, but etched silicon has also recently been used, with excellent noise performance [69]. MCPs with curved microchannels have also been made with a view of reducing ion feedback [70], and microsphere plates have also been made from layers of sintered microspheres [71] and used for TCSPC [72].

The open area ratio is defined as the open area of the MCP pores divided by the total MCP area, and affects the detective quantum efficiency, as photoelectrons that hit the space between channels may be lost. The length to diameter ratio, together with the secondary emission coefficient, determines the gain. The channels are usually tilted on a small angle to the surface ($\sim 8^{\circ}$) to prevent ion feedback. The ions are created by ionisation of residual gas molecules in the tube, an effect that has been studied well in photomultiplier tubes [10]. A particle or photon that enters one of the channels hits its wall due to the bias angle. The impact starts a cascade of electrons that propagates through the channel, which amplifies the original signal by several orders of magnitude depending on the electric field strength and the geometry of the microchannel plate. The MCP channel acts as a continuous dynode (in contrast to discrete dynodes in a PMT, each at a different voltage), which gives it a fast transit time. The positional information where the photon hits the photocathode is preserved because the photocathode is very close to the first MCP, and the phosphor screen, or anode, is very close to the last MCP, a concept termed dual proximity focussing.

MCPs can be used for detecting different types of particles, including electrons, ions and x-rays. Boron-doped MCPs have been used for the detection of neutrons [73–76]. Boron has a high neutron absorption cross section and produces an electron upon absorption of a neutron, which is then multiplied by cascading down the MCP channel in the usual way. For photon detection, a photocathode is placed in front of the MCP. A photon impinging the photocathode liberates a photoelectron, which is accelerated towards the MCP through a high voltage (see figure 5). Most MCP detectors consist of two (chevron configuration) or three (z-stack configuration) MCPs either pressed together or with a small gap between them. The angles of the plates are rotated 180° with respect to each other, minimising ion feedback. One MCP can have gain up to 10 000, but a 3-MCP intensifier can provide gain >10 million. The output electron cloud can then be detected by several methods, depending on the application. If no position read-out is required, the total current can be converted to a voltage via a resistor and read out as a pulse. The transit time is short, and consequently, the transit time spread is also short, 10s of ps. Indeed, MCPs are used as fast detectors for timing in TCSPC, and IRFs of <20 ps have been reported [39]. For wide-field TCSPC, position read-out is necessary, and the electrons can be detected with either a position-sensitive anode, or converted to photons with a phosphor screen and detected with a camera.

MCP detectors do not in principle have 'dead-time' when the detector is not capable of receiving new events, however they can be affected by gain depletion where electrons are not delivered fast enough to an area where many events occur, leading to reduced electron gain and consequently reduced photon event intensity. This can become an issue especially with a fast camera-based read-out which can detect up to 100s of events per frame. With position-sensitive anodes the main factor limiting the count rate is usually the electronics used for the position read-out—for example, the length of the delay line in delay line detectors—which usually limits the count rate to a maximum of one photon per excitation pulse. However, some anode architectures need a higher MCP gain than others for the position read-out, and gain depletion can become a limiting factor with these detectors.

4.1.1. Phosphor + camera readout. In image intensifiers where the required output is the spatial distribution of photons, a phosphor screen is placed behind the last MCP, and the electrons are converted into photons when they hit the phosphor screen. Phosphor screens are commonly used in night vision devices, where the output is viewed by eye. For single photon detection, a 3-stage intensifier can produce up to 10^7 photons from an incoming single photon. These intensified photon events are bright enough to be detected with a normal CCD or CMOS camera, and can, in fact, be observed with the naked eye.

Unlike the pixels in CCD cameras, CMOS pixels have their own amplification, digitization and read-out circuitry. No charge transfer takes place, and all pixels, or rows of pixels, can be read out simultaneously and at very high speeds up to frame rates of MHz. These cameras can be used in combination with an image intensifier for wide-field TCSPC.

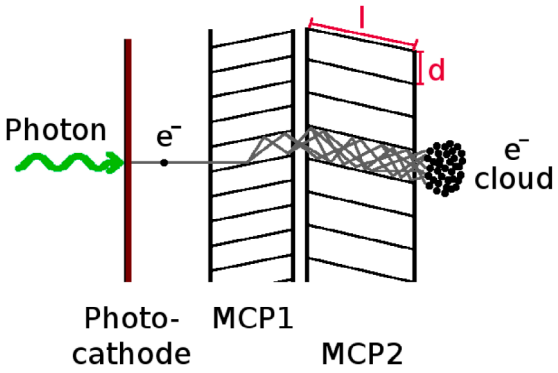

Figure 5. Schematic diagram of the operating principle of an MCP-based detector. A photon impinging the photocathode liberates a photoelectron, which is accelerated towards the first MCP through a high voltage. The electron hits the MCP channel wall due to the bias angle and starts a cascade of electrons which is amplified as it travels through the channel. MCP detectors usually consist of two or three stacked MCPs for higher signal gain. The gain of an MCP depends on the length to diameter ratio (l/d). The output electron cloud has a typical transit time spread Δt_s of a few 10s of ps, so photon arrival time information is preserved.

4.1.1.a. Direct imaging of the photon events. After each excitation pulse, a sequence of frames is acquired during the decay time of the probe, and this process is repeated until enough photons are collected so that a decay histogram is obtained for each pixel of the image, as shown in figure 6(a) [186]. The time resolution of these approaches is limited by the frame rate of the camera—currently 2 MHz with commercially available CMOS cameras—to the microsecond time scale. Although there is a trade-off between a high frame rate and the number of pixels that can be imaged, this technique enables the collection of up to hundreds of photons per frame, and even several photons per pixel after one excitation cycle as long as they arrive in different frames [77]. A similar approach is also used in ion velocity mapping, where molecules in vacuum are ionised by a laser beam, and the arrival time and size of the event can give information about the type of fragment, as reviewed recently [78].

4.1.1.b. Photon arrival timing from the phosphor decay The image intensifier phosphor screen has an afterglow that is usually undesired [79–82]. The phosphor decay time depends on the type of phosphor and can range from nano- to milliseconds, which can cause image artefacts with time-resolved measurements [80]. However, the afterglow can be exploited to find the photon arrival time within the frame exposure time [188]. The principle of obtaining photon arrival time information from the phosphor decay characteristics (figure 6(b)) was demonstrated in 2010 [83]; by matching the phosphor decay with the camera frame rate such that the photon events can be seen in several consecutive frames, the photon arrival time within the exposure time can be found from the relative brightness of the event in different frames. Decay times of phosphorescent beads of ~500 ns have been measured with a P20 phosphor and a 300 kHz camera frame rate [84], but the time resolution could be improved by the combination of a faster phosphor and a higher camera frame rate. A similar

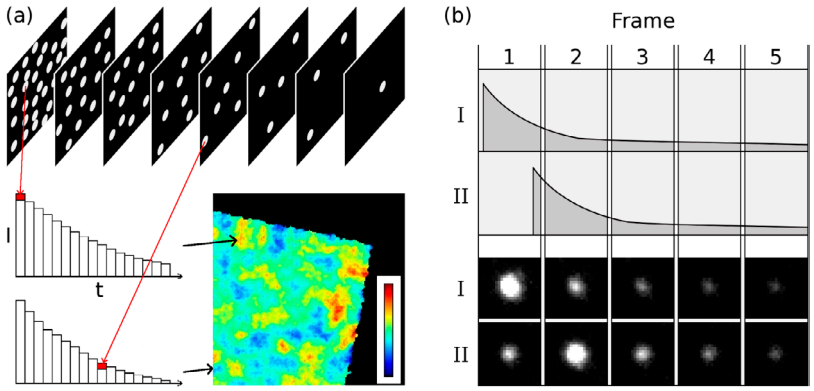

Figure 6. (a) Principle of wide-field TCSPC data acquisition with MCP intensifier and CMOS camera. After each excitation pulse, a sequence of frames is acquired; this process is repeated many times. The location of the photons and the arrival time (frame number) after excitation are extracted by software to build up an arrival time histogram for each pixel of the image, i.e. a 3D data cube in x, y and t. A lifetime image is built by fitting an appropriate exponential decay function to the arrival time histogram in each pixel, and encoding the lifetime in a pseudocolor scale [77, 186]. (b) Time resolution can be improved by using an intensifier with a phosphor that has a longer decay time which allows the photon events to be seen in many consecutive frames. The sample is excited at the beginning of each frame exposure, and the arrival time is found from the relative intensities in the first two frames where the event is detected. Photon I arrives at the beginning of frame 1 and most of the intensity from the phosphor decay is in this frame, whereas for photon II arriving at the end of the frame the second frame is brightest [83, 188]. Reproduced with permission from [179]. Copyright SPIE 2016.

double exposure approach has been used previously for ion velocity mapping, where one [85] or two [86] CCD cameras were used at 25 Hz frame rate.

A characteristic feature of photon counting imaging with MCP / camera combination is the possibility of employing a centroiding technique, where the position of a photon event that covers several pixels can be determined with sub-pixel accuracy [87–104]. The resolution of the image is then not limited by the camera pixel size, but by the MCP pore size and the distribution of the photoelectron trajectories from the photocathode to the first MCP. We have recently demonstrated that software specifically developed for centroiding single-molecule data for super-resolution fluorescence microscopy produces excellent results when applied to centroiding photon events from MCP-based [105] and EBCCD-based camera systems [106].

4.1.2. Anode readout. Instead of using a phosphor to convert the electrons from the MCP into photons, the electrons can be read out with a position-sensitive anode. With this approach, the arrival time of the photon is obtained directly from the MCP, with picosecond time resolution.

The earliest implementation of a 2D resistive anode readout consisted of a square sheet of insulating material with resistivity coating and a contact at each corner. The pulse amplitudes and rise-times are proportional to the event distance from the contact, and the event location can be determined from either the charge division or the difference in the signal timing between opposing contacts [64, 65]. This design required a stack of 5 MCPs to produce sufficient gain, and the signals were processed in the hardware. The first design suffered from many drawbacks, such as poor spatial resolution, nonlinearity across the anode, fixed pattern noise from the signal digitization, and variation in resolution due to a wide pulse height distribution. Some characteristics were improved by an optimised design of the MCP stack, the anode and the signal processing electronics and arithmetic [107]. Others, however, such as slow event processing rate (i.e. low count rate) and scaling for larger area detectors, are difficult to improve with this type of anode architecture.

More sophisticated, accurate and sensitive read-out architectures were developed subsequently. They can be divided into charge division anodes where the position is obtained from the relative charge amplitudes in different anodes, and propagative / delay line anodes where the position is obtained from the propagation time of the pulse along a delay line. Many different geometries exist, some of which have been used for TCSPC:

- In a **delay line anode** (figure 7(a)) the electron cloud is detected by meandering wires inside the intensifier tube or LC elements on a printed circuit board placed outside of the intensifier. The resulting pulse travels to both ends of the delay line, and the position is obtained from the propagation time difference of the signal to the ends of the delay line. Different geometries have been designed [108, 109], and the event detection rate is usually limited by the signal propagation time to the ends of the delay line.
- A **cross-strip anode** (figure 7(b)) has many strips in both x and y direction, all of which are read out; the coarse event position is obtained from the strip with highest charge, and the centroid position can be calculated with sub-strip accuracy from the charge distribution on the neighbouring strips [110, 111]. An amplifier is required for each strip, but this geometry allows higher event detection rate than a delay line anode as several photons can be detected in one excitation cycle [112, 113].
- In a **quadrant anode** [114] (figure 7(d)) the anode is divided into quarters and placed behind the MCPs, such that for each photon event part of the electron cloud hits each of the four quadrants. The event position can then be calculated from relative amounts of charge collected by each quadrant. Some designs have a ring-shaped fifth

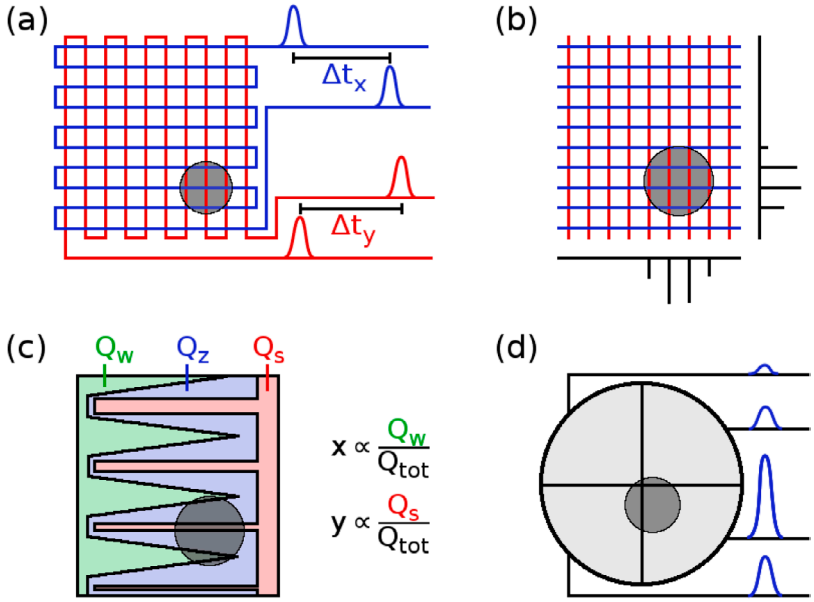

Figure 7. Some different position-sensitive read-out anode architectures. (a) In a delay line anode, the position is obtained from the signal propagation-time difference to the ends of the wire; (b) cross-strip anode where all strips are read out and the position obtained from the charge distribution; (c) wedge-and-strip anode where the position is calculated from the relative charge of the components; and (d) quadrant anode where the position is obtained from the relative charge in the four quadrants.

anode around the detector inside to help spread out the electron cloud over the four anodes [115–117].

- A **wedge-and-strip anode** (figure 7(c)) has three read-outs: the relative charge in the wedge is related to event position in the direction parallel to the wedges, and the strips are not of equal width and thus the charge collected by the strip anode can be used for the calculation of the event position in the direction perpendicular to the strips [118, 119].

Other read-out architectures exist [120–122], most of them originally developed for astronomical applications. The main drawback of these types of anodes is that, except for the cross strip anode, they typically detect only one photon per pulse for the whole field of view. Advanced read-out architectures that are able to resolve multi-photon hits have been designed [123], however they do not fundamentally solve the problem that the count rate is limited by the position read-out electronics rather than the need to avoid overlapping events.

4.1.3. Pixel array readout. Similar to cameras, detector arrays [40, 124, 125] and pixelated read-out anodes allow the positions of the events from the detector to be read out directly at each pixel. An 8×8 pixel anode read-out with 43 ps time resolution that uses application specific integrated circuits (ASICs) originally developed in CERN has been demonstrated, and a 32×32 pixel detector has been planned, but the large pixel size of 0.5 mm and limited number of pixels mean that the development of these detectors is aimed more at high-content screening applications [126]. Another CMOS pixel read-out chip (also developed in CERN for particle physics applications), the MediPix2/TimePix ASIC with 10 ns time resolution, 256×256 pixels and 55 μm pixel size, has been combined with an MCP for single photon detection [127, 128]. The main drawback of this detector is the 266 μs frame read-out time which limits the global count rate. Although these chips are capable of high timing resolution, so far they have found more applications in photon counting imaging where the arrival timing of the photons is not required and the photons can be accumulated in each pixel before the frame read-out. However, new generation Timepix3 chips [129] improve the timing resolution by an order of magnitude to 1.5 ns and allow asynchronous readout of the hit pixels with only 0.5 μs dead time, effectively allowing multi-hit functionality at the pixel level. Combined with a faster read-out in the kHz regime [128], these detectors could soon find more applications in wide-field TCSPC imaging.

4.2. SPAD arrays

A SPAD is a reverse biased semiconductor p-n junction operating with a bias voltage above the breakdown voltage where a single photon (or a single dark current electron) can set off a significant avalanche of electrons. Single SPADs were first used for fast timing applications in the 1980s [130, 131], and the implementation of SPADs in CMOS technology in 2003 enabled the development of SPAD arrays [132]. In the past decade a number of SPAD array image sensors have been developed, which simultaneously deliver single photon sensitivity, tens of thousands of pixels spatial resolution and picosecond timing resolution [57, 133, 134].

One advantage of SPAD arrays is that each pixel can perform TCSPC independently with a low dead time and consequently high count rate per pixel, yielding enormous overall count rates of GHz [135]. A 256×256 TAC imager has been described [136] and 340×96 SPAD arrays also exist [137], and it is only a question of time until these huge advantages are leveraged for FLIM. However, SPAD array detectors currently have a small fill factor ($<10\%$), because the majority of the area of each pixel is occupied by electronic circuits

to perform the timing, with only a small light-sensitive area dedicated to the detection of photons. SPAD line sensors place pulse processing electronics below the detectors [138, 139], thus allowing a high fill-factor, but this is currently not available for 2D array detectors. One promising solution for improving the light detection efficiency is to use a microlens array in front of the detector to focus the fluorescence signal onto the light-sensitive area [140, 141].

The noise levels of SPAD arrays are much higher than for MCP-based detectors. The dark noise performance of SPAD arrays, typically 100s of counts per pixel (SPAD), depending on the operating voltage and temperature [57], can be improved to 10s of counts per pixel (25 Hz has been quoted [142]) but it is still many orders of magnitude higher than MCP-based intensifiers, for which 0.02 events/s/cm^2 have been quoted [143]. This consideration gains in importance as the detection window and lifetime to be measured increases, and the count rate drops. It is also an important point to consider when enlarging the size of the light sensitive area in SPADs, as the dark noise increases with the area [57].

Recently a 32-channel TCSPC system has been developed employing the hybrid integration of a custom 32 SPAD array with 32-channel active quench and time to analogue converter array [144]. The design of detectors and timing electronics on a single substrate provides compactness and large numbers of channels but compromises fill-factor and SPAD performance (jitter, photon detection efficiency, afterpulsing and dark count). However, this detector has a time-to-digital converter (TDC) in each pixel with 55 ps resolution, allowing independent TCSPC in each pixel of a 32×32 pixel array simultaneously.

Advanced SPAD array manufacturing techniques such as 3D stacking are expected to push fill-factor and spatial resolution to comparable levels to incumbent technologies such as sCMOS or EMCCD whilst offering picosecond time resolution. Recent developments in CMOS SPAD technology have shown significant improvements in many features [145], such as the dead time [146], dark count [142, 147], pixel miniaturization [148], and quantum efficiency in the longer wavelength region [149]. It is expected high resolution CMOS SPAD arrays for ranging applications (Geiger mode light detection and ranging (LIDAR)) [137, 150] will soon be applied to FLIM.

4.3. Superconducting detectors

Superconducting tunnel junction (STJ), kinetic induction detectors (KID) and superconducting nanowire single photon detectors (SNSPD) as well as transition edge sensors (TES) go beyond the principles employed in semiconductor and photoelectronic vacuum devices, i.e. electron–hole pair generation and the photoelectric effect, exploiting superconductivity instead. They have been developed and used for astronomical applications, as reviewed recently [151], but some of these detectors have also been used for the detection of instrumental responses of laser pulses and fluorescence decays via TCSPC [152, 153].

While transition edge sensors are calorimeters that detect the energy of a photon deposited in the detector via a rise in temperature, STJ detectors have superconducting photocathodes and rely on the photons separating the individual electrons in Cooper pairs which only have a milli-electronvolt binding energy [154]. The resulting electrons tunnel through a thin layer beyond which they are picked up and amplified. KIDs detect photons by shifting the frequency of a superconducting LCR oscillator upon photon absorption, which can be detected with great sensitivity.

An interesting feature of these detectors (STJ, KID and TES) is that they have an intrinsic wavelength resolution—the detector can determine the wavelength of the detected photon without employing any filters, gratings or prisms to disperse the light. In the case of STJs, this is given by the pulse height of the signal, i.e. the number of electrons generated by an incident photon. Moreover, they have a high quantum efficiency over a very large wavelength range from x-rays to infra-red and low noise, but they need to be operated at liquid helium temperatures, i.e. below −270 °C in the milli-Kelvin regime. These devices have already been demonstrated to be able to measure the spectra of fluorescent dyes in solution [155] and as labels for DNA [156], but they have not been used for microscopy. The disadvantage is that they have a very long pulse rise time of micro- or milliseconds, so count rates in a single pixel are limited. Although pixellated devices have been manufactured and used on telescopes for optical astronomy at infrared wavelengths [157], the readout of many pixels is a challenging task.

SNSPDs, on the other hand, have a very fast pulse rise time and can count single photons at MHz count rates [152, 158]. They also have very low noise, but limited quantum efficiencies (which can be overcome by cavity resonators [159]) and no intrinsic wavelength resolution. They are based on meandering superconducting wires just below the transition temperature, as reviewed recently [160]. A photon deposits energy, heats up the wire so that the transition temperature is exceeded, and a pulse results. They have an excellent signal-to-noise ratio in the infrared and picosecond IRFs when combined with TCSPC [153]. They have recently been employed to detect singlet oxygen luminescence at 1270 nm, generated by photosensitizer rose Bengal, with unprecedented sensitivity [161]. Although these devices have not yet been applied to fluorescence microscopy, and detector development is aimed more towards infrared wavelengths used in optical communications, parallelised detectors have been built [162] and there have been recent developments towards large-area arrays [163].

4.4. Overview of wide-field TCSPC techniques

A summary of different wide-field TCSPC techniques is shown in table 1. Currently most wide-field TCSPC methods are based on an MCP image intensifier to amplify the photon signal, in combination with a position sensitive detector. Timing read-out from the MCP allows the photon arrival to be determined with picosecond accuracy, and different position-sensitive read-out anodes determine the photon position, typically based on a pulse propagation time or charge division principle. The combination of a phosphor screen and an ultrafast frame-rate CMOS camera allows up to 100s of photons to be detected simultaneously after one excitation pulse, but the timing accuracy of this method is limited by the camera frame rate to microsecond time scale. Fluorescence super-resolution

Table 1. Summary of wide-field TCSPC techniques.

Method	Advantages	Disadvantages
MCP + Camera read-out	100s of photons / excitation pulse High fill factor, low noise Large area, several cm diameter	Limited to μs time resolution High voltage required MCP lifetime limited by total charge that can be extracted
MCP + Anode read-out	*ps* time resolution High fill factor, low noise 18 to 40 mm diameter	Max 1 photon / excitation pulse Limited global count rate High voltage required MCP lifetime limited by total charge that can be extracted
MCP + Pixel array read-out	100s of photons / excitation pulse High fill factor, low noise Each pixel counts independently	Limited to *ns* time resolution Limited global count rate High voltage required MCP lifetime limited by total charge that can be extracted
SPAD array	*ps* time resolution High global count rate Each pixel counts independently	Limited array size Low fill factor, high noise Non-uniformity across array Small overall size
STJ array	Wide wavelength range Intrinsic wavelength resolution low noise	Operation temperature < -270 °C Slow, μs pulse rise time →Low global count rate
SNSPD array	Fast pulse rise time →High count rate low noise	Low operation temperature

software can be used to centroid photon events to sub-pixel accuracy [105, 106]. MCPs are fundamentally limited by their count-rate in the MHz region, and their lifespan is limited by the overall amount of charge that can be extracted from the channels. They have a very low noise, but the quantum efficiency of conventional photocathodes is limited. They can be manufactured with large diameters [164], but the photoelectronic vacuum technology is a drawback compared to silicon-based solid state technology.

SPAD arrays are a relatively new development in wide-field TCSPC, and while their current use as cameras is limited by technical issues, continuing development in this field may enable high count rate picosecond wide-field TCSPC soon [135]. Work in this rapidly evolving field is underway to reduce noise, manufacture large arrays with single photon sensitivity and picosecond timing abilities, as well as large fill factors.

Single-point superconducting detectors have been used to detect fluorescence spectra in the visible [155, 156] and the decay of sensitised singlet oxygen signals at 1270 nm [161]. Superconducting detectors are still a new and growing technology, and their combination with scanning microscopy to produce images, or the use of pixellated devices for time-resolved wide-field microscopy would be interesting.

5. Applications of wide-field TCSPC

Wide-field TCSPC techniques find many applications in FLIM: the low excitation power used is especially beneficial for observing dynamics in living cells over long periods, while wide-field data collections allows particle tracking, and techniques that enable the collection of many photons per excitation pulse speed up the data collection time for long lifetime measurements.

5.1. Low light level wide-field FLIM

The excitation power required for wide-field single photon counting is typically very low, of the order of microwatts, and evenly distributed over the field of view, avoiding high local illumination intensities. For example, 1 μW excitation power over a 100×100 μm field of view corresponds to 10 mW cm^{-2}, an order of magnitude less than the sun's irradiance of the earth, 100 mW cm^{-2}. A confocal microscope uses a similar excitation power, but concentrated in the focal spot of the objective, leading to a high local intensity in the order of 100 W cm^{-2}. Multiphoton microscopy requires several orders of magnitude more power, often in the order of MW cm^{-2} to GW cm^{-2}.

Wide-field FLIM is useful for monitoring cell dynamics, where the low illumination intensity allows long-term monitoring of living cells. Quadrant anodes, which are commercially available, have been applied to FLIM of biological samples [165] to the study of protein–protein interaction by FRET [166–169] and photosynthesis research, which is very sensitive to the excitation power [170].

5.2. Dynamics and single-particle tracking

Wide-field FLIM enables single-particle tracking measurements, where the whole-field data collection allows the tracking of individual molecule or particle trajectories. As each photon has two time stamps—one for the arrival time since the excitation pulse and one for the time since the start of the

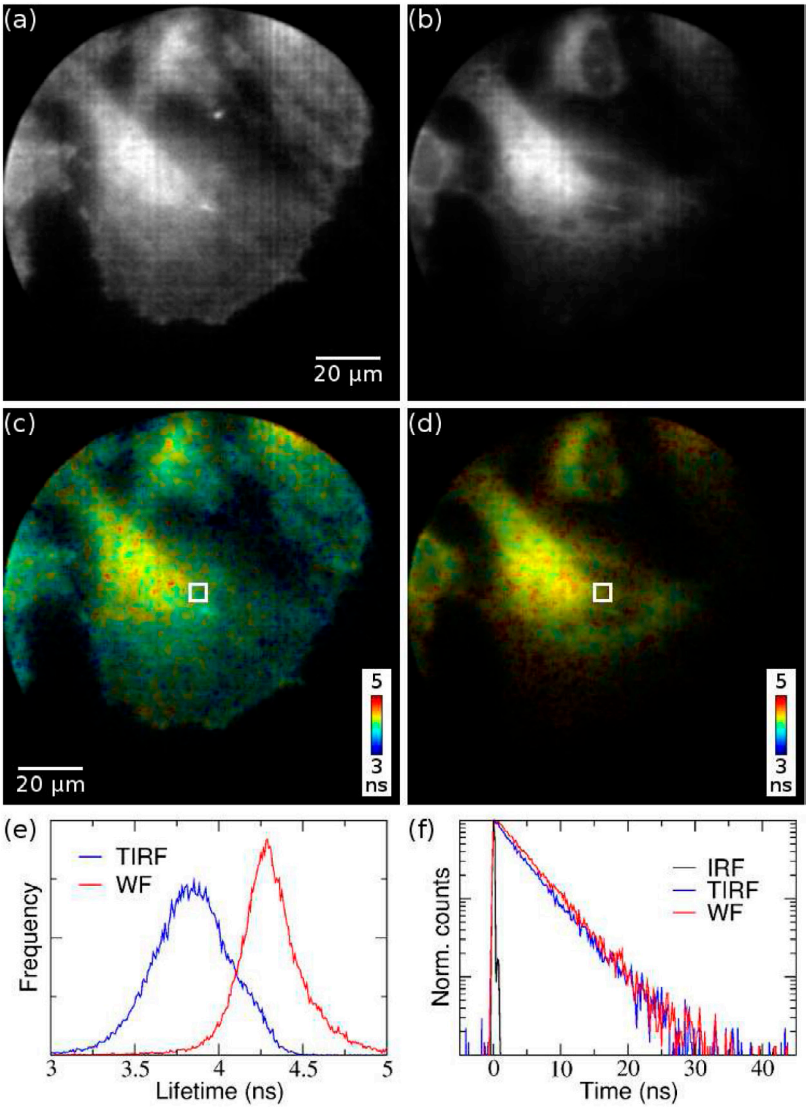

Figure 8. Wide-field TCSPC images of HeLa cells acquired with a delay line detector. The measured intensity shows the cell membrane only under TIRF illumination (a), and lifetime is shorter (c), while the whole cell is visible under wide-field illumination (b) and the lifetime is longer (d). (e) Histogram of the individual pixel lifetimes in ((c), (d)). (f) Fluorescence decays in the area indicated by a white rectangle in ((c), (d)). Reproduced from [179].

experiment—the data can be divided into time frames of suitable duration that allows the tracking of the molecules but also enough photons in each frame for lifetime fitting. Single-quantum dot tracking and FLIM has been demonstrated with an MCP-based delay line anode detector [171], and quadrant anodes have been applied to FLIM of mitochondrial transport in neuronal processes [168].

5.3. Specialised microscopy techniques

Wide-field TCSPC is especially useful for microscopy techniques where excitation beam scanning is not possible, or cumbersome, and the whole field of view is illuminated with a technique that provides depth discrimination. One of these techniques is total internal reflection fluorescence (TIRF) microscopy. In objective-based TIRF, the excitation light is reflected back from the coverslip, and the sample is excited by an evanescent wave only near (up to ∼100 nm) the coverslip. TIRF-FLIM has been demonstrated with quadrant anodes [172], SPAD array detectors [173], and delay line anodes (see figure 8) [174]. A similar technique is supercritical angle fluorescence (SAF) microscopy where whole sample is excited but the light is collected only from high angles near the coverslip [175, 176].

Lightsheet microscopy, also called selective/single plane illumination microscopy (SPIM) and named Nature Methods 'Method of the Year' 2014, uses a 2nd objective to illuminate the focal plane of the sample with a sheet of light at an angle of 90° relative to the imaging objective, thus providing optical sectioning and reducing photobleaching outside the focal plane. Lightsheet microscopy has been combined with FLIM using frequency domain [177] and gating-scanning methods [178], but wide-field TCSPC would allow a more sensitive and precise lifetime measurement, combined with lower excitation intensity.

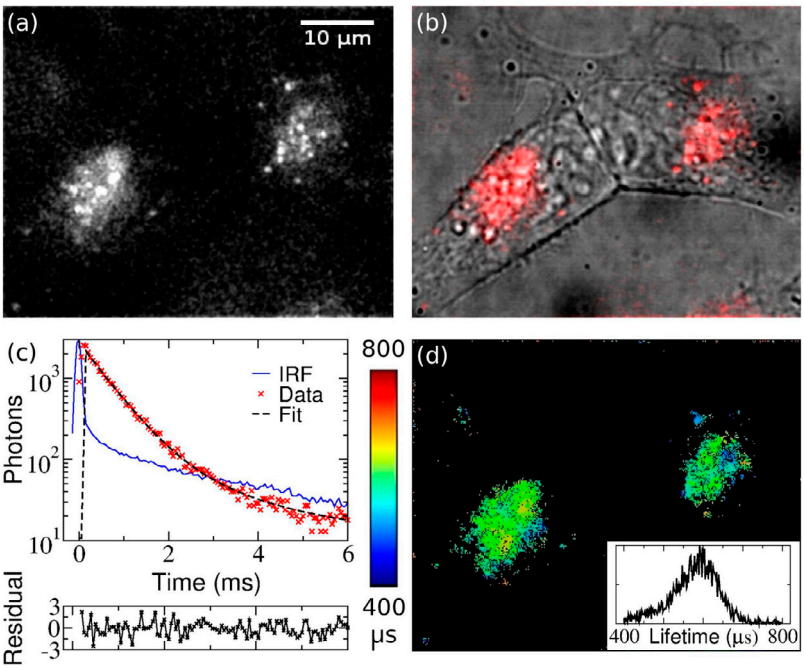

Figure 9. Images of 40 nm europium beads in living HeLa cells obtained by MCP + fast camera wide-field TCSPC. (a) Wide-field TCSPC intensity and (b) composite transmission (gray) and intensity (red). (c) Biexponential fit to all pixels in (a) yields a europium lifetime of 570 ± 9 μs (and a 2.0 ms background component, see IRF). (d) Lifetime image (acquisition time 3.5 s); inset shows a lifetime histogram of all individual pixel lifetime values. Reproduced with permission from [186]. Copyright OSA 2014.

5.4. Long lifetime measurements

Some wide-field TCSPC techniques are especially well suited for measuring phosphorescence lifetimes in the micro- and millisecond time region—a techinque known as phosphorescence lifetime imaging (PLIM). In life sciences, PLIM is often used to image microenvironment of the probe, such as the oxygen concentration or viscosity [180, 181]. The long lifetime increases the sensitivity by giving the probe more time to interact with the environment, and it allows the short-lived autofluorescence from the sample to be discarded. Phosphorescence anisotropy measurements can also be used to study the rotational diffusion of large proteins, whose movement is too slow to be measured with fast fluorescence decays [182, 183]. Besides life sciences, PLIM has been used to study air-flow and pressure in aerodynamic studies [184], and for temperature measurements in industrial thermometry applications [185].

Camera-based wide-field TCSPC is especially well suited for PLIM, where scanning a single spot over the image would lead to very long image acquisition times. Pile-up restrictions of most other detectors limit the count rate such that approximately 1 in 100 pulses yields a photon, but this technique enables the collection of hundreds of photons per excitation cycle—even several photons after one excitation cycle per pixel, as long as they arrive in different frames [77]. This shortens the data acquisition time with long lifetime probes, such as lanthanides which have lifetimes in the millisecond regime, and has been demonstrated in living cells labelled with 40 nm Europium beads, as shown in figure 9 [186]. With current camera frame rates of around 1 MHz, this technique allows the measurement of lifetimes down to ∼1 μs. The measurement of the arrival time from the photon event phosphor decay can improve the time resolution beyond the inverse frame rate of the camera, and the slower frame rate used for this technique also increases the number of recorded pixels, thus allowing a bigger field of view. Lifetimes around 1 μs have been measured with several transition metal probes using a 54 kHz frame rate, including a ruthenium based oxygen sensor in living cells [187, 188], and a lifetime of ∼500 ns has been measured with a 300 kHz camera frame rate [84].

5.5. Other applications

Besides fluorescence microscopy, wide-field TCSPC detectors have applications in diverse fields of science and technology. Optical communications (on earth [162], near earth [189], and in deep space [32, 190]), quantum cryptography and light detection and ranging (LIDAR) [191, 192] techniques use wide-field photon counting detectors, and the recent advances especially in superconducting detector and SPAD array technology can be attributed to the rapidly expanding applications in these fields. Although the wavelengths used in these applications are usually in the infrared, other requirements from the detector, such as picosecond time resolution and low noise, are similar to fluorescence microscopy.

In addition to visible light, single photon detectors based on optoelectronic vacuum devices can also detect other types of electromagnetic radiation, including UV photons, x-rays and gamma rays, as well as particles, such as electrons, neutrons and ion fragments. MCPs are used in time-of-flight mass spectroscopy for detecting ion fragments [78, 193], while boron-doped MCPs have been used for neutron detection [73–76], where timing of the neutron events allows distinction of cold and thermal neutrons, and thus allows simultaneous imaging at different

neutron energies. In autoradiography, MCPs are used for detecting decay emissions from radioactively labelled samples [194, 195]. We note that for these approaches, once a particle has been converted into an electron in the MCP, the detection process is the same as for photons—and the development of wide-field detectors for FLIM may also benefit these applications.

6. Conclusion

FLIM is a widely used imaging technique in the life sciences which allows the monitoring of the microenvironment of fluorophores and their interaction. Wide-field TCSPC FLIM combines the unique advantages of single photon sensitivity and accuracy with wide-field data collection. This is particularly relevant for various microscopy methods employing cameras, not beam scanning, and wide-field TCSPC detectors allow single photon sensitive FLIM to be performed with these microscopy methods. TCSPC has the best signal-to-noise ratio of the standard time-resolved imaging methods, and is accurate enough to allow multi-exponential fluorescence lifetime fitting. The extremely low illumination intensity, distributed evenly over the field of view, is beneficial especially in life science applications where it allows long-term monitoring of living cells and organisms, while wide-field data collection enables the observation of cell dynamics and single-particle tracking.

In other fields of science and technology, the development of wide-field TCSPC will also benefit methods where single photon time-of-flight measurements are required, for example Geiger mode LIDAR [191, 192], ion velocity mapping [78, 85, 86] or photon correlation techniques [196]. Many wide-field TCSPC methods are currently based on MCPs, a mature technology used especially in astronomy and medical imaging, but there is a trade-off between count rate and time resolution. Recent developments of SPAD arrays in CMOS technology, as well as advances in superconducting detector technology, show great promise for high count rate picosecond wide-field TCSPC, single photon sensitive FLIM in the infra-red and generally single-photon sensitive FLIM of microscopy methods employing cameras.

Acknowledgments

We would like to thank the UK's Medical Research Council (MRC) for funding.

References

[1] Einstein A 1905 Über einen die Erzeugung und Verwandlung des Lichtes betreffenden heuristischen Gesichtspunkt *Ann. Phys.* **322** 132–48
Einstein A 1965 *Am. J. Phys.* **33** 367–74 (Engl. transl.)
[2] Lewis G N 1926 The conservation of photons *Nature* **118** 874–5
[3] Roychoudhuri C, Kracklauer A F and Creath K 2008 *The Nature of Light: What is a Photon?* (Boca Raton, FL: CRC Press)
[4] Hertz H 1887 Ueber einen Einfluss des ultravioletten Lichtes auf die electrische Entladung *Ann. Phys.* **267** 983–1000
[5] Austin L and Starke H 1902 Ueber die Reflexion der Kathodenstrahlen und eine damit verbundene neue Erscheinung secundärer Emission *Ann. Phys.* **314** 271–92
[6] Iams H and Salzberg B 1935 The secondary emission phototube *Proc. IRE* **23** 55–64
[7] Kubetsky L A 1937 Multiple amplifier *Proc. IRE* **25** 421–33
[8] Zworykin V K, Morton G A and Malter L 1936 The secondary emission multiplier-a new electronic device *Proc. IRE* **24** 351–75
[9] Allen J S 1939 The detection of single positive ions, electrons and photons by a secondary electron multiplier *Phys. Rev.* **55** 966–71
[10] Hungerford G and Birch D J S 1996 Single-photon timing detectors for fluorescence lifetime spectroscopy *Meas. Sci. Technol.* **7** 121–35
[11] Bothe W and Kolhörster W 1929 Das Wesen der Höhenstrahlung *Z. Phys.* **56** 751–77
[12] Rossi B 1930 Method of registering multiple simultaneous impulses of several Geiger's counters *Nature* **125** 636
[13] Rossi B and Nereson N 1942 Experimental determination of the disintegration curve of mesotrons *Phys. Rev.* **62** 417–22
[14] Bell R E, Graham R L and Petch H E 1952 Design and use of a coincidence circuit of short resolving time *Can. J. Phys.* **30** 35–52
[15] Pike E R 2010 Lasers, photon statistics, photon-correlation spectroscopy and subsequent applications *J. Eur. Opt. Soc.-Rapid* **5** 10,047S
[16] Bollinger L M and Thomas G E 1961 Measurement of the time dependence of scintillation intensity by a delayed-coincidence method *Rev. Sci. Instrum.* **32** 1044–50
[17] Bachrach R Z 1972 A photon counting apparatus for kinetic and spectral measurements *Rev. Sci. Instrum.* **43** 734–7
[18] Binkert Th, Tschanz H P and Zinsli P E 1972 The measurement of fluorescence decay curves with the single-photon counting method and the evaluation of rate parameters *J. Lumin.* **5** 187–217
[19] Lewis C 1973 The measurement of short-lived fluorescence decay using the single photon counting method *Rev. Sci. Instrum.* **44** 107–14
[20] Birch D J S and Imhof R E 1981 Coaxial nanosecond flashlamp *Rev. Sci. Instrum.* **52** 1206–12
[21] Phillips D 2016 A lifetime in photochemistry; some ultrafast measurements on singlet states *Proc. R. Soc.* A **472** 20160102
[22] Bugiel I, König K and Wabnitz H 1989 Investigation of cells by fluorescence laser scanning microscopy with subnanosecond time resolution *Lasers Life Sci.* **3** 47–53
[23] Becker W, Bergmann A, Hink M A, König K, Benndorf K and Biskup C 2004 Fluorescence lifetime imaging by time-correlated single-photon counting *Microsc. Res. Tech.* **63** 58–66
[24] Buller G S and Collins R J 2010 Single-photon generation and detection *Meas. Sci. Technol.* **21** 012,002
[25] Hadfield R H 2009 Single-photon detectors for optical quantum information applications *Nat. Photon.* **3** 696–705
[26] Eisaman M D, Fan J, Migdall A and Polyakov S V 2011 Single-photon sources and detectors *Rev. Sci. Instrum.* **82** 071,101
[27] O'Connor D V and Phillips D 1984 *Time-Correlated Single-Photon Counting* (New York: Academic)
[28] di Serego Alighieri S, Perryman M A C and Macchetto F 1985 The ESA photon counting detector—a scientific model for the faint object camera *Astron. Astrophys.* **149** 179–85
[29] Kröger H W, Schmidt G K and Pailer N 1992 Faint object camera: European contribution to the Hubble space telescope *Acta Astronaut.* **26** 827–34
[30] Longdon N 1990 A long look back: ESA's faint object camera. The story of the faint object camera, one of ESA's contributions to the Hubble space telescope (European Space Agency Publications Division)
[31] Previte M J R *et al* 2015 DNA sequencing using polymerase substrate-binding kinetics *Nat. Commun.* **6** 6936

[32] Hemmati H 2007 Interplanetary laser communications *Opt. Photonics News* **18** 22–7
[33] Seitz P and Theuwissen A J P 2011 *Single Photon Imaging* (Heidelberg: Springer)
[34] Bevington P R and Robinson D K 2003 *Data Reduction and Error Analysis for the Physical Sciences* (New York: McGraw-Hill)
[35] Felekyan S, Kühnemuth R, Kudryavtsev V, Sandhagen C, Becker W and Seidel C A M 2005 Full correlation from picoseconds to seconds by time-resolved and time-correlated single photon detection *Rev. Sci. Instrum.* **76** 083104
[36] Wahl M, Rahn H-J, Gregor R I, Erdmann R and Enderlein J 2007 Dead-time optimized time-correlated photon counting instrument with synchronized, independent timing channels *Rev. Sci. Instrum.* **78** 0331066
[37] Wahl M 2015 Modern TCSPC electronics: principles and acquisition modes *Advanced Photon Counting* (Berlin: Springer) pp 1–21
[38] James D R and Ware W R 1986 Recovery of underlying distributions of lifetimes from fluorescence decay data *Chem. Phys. Lett.* **126** 7–11
[39] Becker W 2005 *Advanced Time-Correlated Single Photon Counting Techniques* (Berlin: Springer)
[40] Suhling K, McLoskey D and Birch D J S 1996 Multiplexed single-photon counting. II. The statistical theory of time-correlated measurements *Rev. Sci. Instrum.* **67** 2238–46
[41] Istratov A A and Vyvenko O F 1999 Exponential analysis in physical phenomena *Rev. Sci. Instrum.* **70** 1233–57
[42] Liu M, Jia M, Pan H, Li L, Chang M, Ren H, Argoul F, Zhang S and Xu J 2014 Instrument response standard in time-resolved fluorescence spectroscopy at visible wavelength: quenched fluorescein sodium *Appl. Spectrosc.* **68** 577–83
[43] Birch D J S and Imhof R E 1999 Time-domain fluorescence spectroscopy using time-correlated single-photon counting *Topics in Fluorescence Spectroscopy: Techniques* (Berlin: Springer) pp 1–95
[44] Fischer R S, Wu Y, Kanchanawong P, Shroff H and Waterman C M 2011 Microscopy in 3D: a biologist's toolbox *Trends Cell Biol.* **21** 682–91
[45] Nobel Media AB 2014 The Nobel prize in chemistry 2014 (http://www.nobelprize.org/nobel_prizes/chemistry/laureates/2014/)
[46] Nobel Media AB 2009 The Nobel prize in physics 2009 (http://www.nobelprize.org/nobel_prizes/physics/laureates/2009/)
[47] Smith G E 2009 The invention and early history of the CCD *Nucl. Instrum. Methods Phys. Res.* A **607** 1–6
[48] Becker W 2012 Fluorescence lifetime imaging—techniques and applications *J. Microsc.* **247** 119–36
[49] Berezin M Y and Achilefu S 2010 Fluorescence lifetime measurements and biological imaging *Chem. Rev.* **110** 2641–84
[50] Borst J W and Visser A J W G 2010 Fluorescence lifetime imaging microscopy in life sciences *Meas. Sci. Technol.* **21** 102002
[51] Suhling K *et al* 2015 Fluorescence lifetime imaging (FLIM): basic concepts and some recent developments *Med. Photonics* **27** 3–40
[52] Esposito A, Gerritsen H C and Wouters F S 2007 Optimizing frequency-domain fluorescence lifetime sensing for high-throughput applications: photon economy and acquisition speed *J. Opt. Soc. Am.* A **24** 3261–73
[53] Philip J and Carlsson K 2003 Theoretical investigation of the signal-to-noise ratio in fluorescence lifetime imaging *J. Opt. Soc. Am.* A **20** 368–79
[54] Gratton E, Breusegem S, Sutin J, Ruan Q and Barry N 2003 Fluorescence lifetime imaging for the two-photon microscope: time-domain and frequency-domain methods *J. Biomed. Opt.* **8** 381–90
[55] Zhao Q, Young I T and de Jong J G S 2011 Photon budget analysis for fluorescence lifetime imaging microscopy *J. Biomed. Opt.* **16** 086007–16
[56] Amos W B and White J G 2003 How the confocal laser scanning microscope entered biological research *Biol. Cell* **95** 335–42
[57] Charbon E 2014 Single-photon imaging in complementary metal oxide semiconductor processes *Phil. Trans. R. Soc.* A **372** 20130100
[58] Stepanov S, Bakhlanov S, Drobchenko E, Eckert H-J and Kemnitz K 2010 Widefield TSCSPC-systems with large-area-detectors: application in simultaneous multi-channel-FLIM *Proc. SPIE* **7376** 73760Z–20
[59] Hartig R, Prokazov Y, Turbin E and Zuschratter W 2014 Wide-field fluorescence lifetime imaging with multi-anode detectors *Methods Mol. Biol.* **1076** 457–80
[60] Sharp N A 1992 Millisecond time resolution with the Kitt peak photon-counting array *Publ. Astron. Soc. Pac.* **104** 263–9
[61] Farnsworth P T 1934 Electron multiplier *US Patent* 1969399
[62] Wiley W C and Hendee C F 1962 Electron multipliers utilizing continuous strip surfaces *IRE Trans. Nucl. Sci.* **9** 103–6
[63] Goodrich G W and Wiley W C 1962 Continuous channel electron multiplier *Rev. Sci. Instrum.* **33** 761
[64] Augustyniak W M, Brown W L and Lie H P 1972 A hybrid approach to two dimensional charged particle position sensing preserving energy resolution *IEEE Trans. Nucl. Sci.* **19** 196–200
[65] Lampton M 1974 The Ranicon: a resistive anode image converter *Rev. Sci. Instrum.* **45** 1098–105
[66] Martindale A, Lapington J S and Fraser G W 2007 Photon counting with small pore microchannel plates *Nucl. Instrum. Methods Phys. Res.* A **573** 111–4
[67] Siegmund O H W, Vallerga J V, Tremsin A S, McPhate J, Michalet X, Colyer R A and Weiss S 2011 Microchannel plate imaging photon counters for ultraviolet through NIR detection with high time resolution *Proc. SPIE* **8033** 80330V–12
[68] Siegmund O H W 2004 High-performance microchannel plate detectors for UV/visible astronomy *Nucl. Instrum. Methods Phys. Res.* A **525** 12–6
[69] Franco A, Geissbühler J, Wyrsch N and Ballif C 2014 Fabrication and characterization of monolithically integrated microchannel plates based on amorphous silicon *Sci. Rep.* **4** 4597
[70] Boutot J P, Eschard G, Polaert R and Duchenois V 1976 A microchannel plate with curved channels: an improvement in gain relative variance and ion noise for channel plate tubes *Adv. Electron. Electron Phys.* **40A** 103–11
[71] Tremsin A S, Pearson J F, Lees J E and Fraser G W 1996 The microsphere plate: a new type of electron multiplier *Nucl. Instrum. Methods Phys. Res.* A **368** 719–30
[72] Rosenwaks Y 1997 Microsphere electron multiplier applicability to picosecond time correlated single photon counting *Rev. Sci. Instrum.* **68** 2911–2
[73] Fraser G W and Pearson J F 1990 The direct detection of thermal neutrons by imaging microchannel plate detectors *Nucl. Instrum. Methods Phys. Res.* A **293** 569–74
[74] Siegmund O H, Vallerga J V, Tremsin A S, McPhate J and Feller B 2007 High spatial resolution neutron sensing microchannel plate detectors *Nucl. Instrum. Methods Phys. Res.* A **576** 178–82
[75] Tremsin A S, McPhate J B, Vallerga J V, Siegmund O H W, Hull J S, Feller W B and Lehmann E 2009 Detection efficiency, spatial and timing resolution of thermal and cold neutron counting MCP detectors *Nucl. Instrum. Methods Phys. Res.* A **604** 140–3

[76] Tremsin A S, McPhate J B, Vallerga J V, Siegmund O H W, Feller W B, Lehmann E, Kaestner A, Boillat P, Panzner T and Filges U 2012 Neutron radiography with sub-15 micron resolution through event centroiding *Nucl. Instrum. Methods Phys. Res.* A **688** 32–40

[77] Sergent N, Levitt J A, Green M and Suhling K 2010 Rapid wide-field photon counting imaging with microsecond time resolution *Opt. Express* **18** 25292–8

[78] Vallance C *et al* 2014 Fast sensors for time-of-flight imaging applications *Phys. Chem. Chem. Phys.* **16** 383–95

[79] Mainprize J G and Yaffe M J 1998 The effect of phosphor persistence on image quality in digital x-ray scanning systems *Med. Phys.* **25** 2440–54

[80] vandeVen M, Ameloot M, Valeur B and Boens N 2005 Pitfalls and their remedies in time-resolved fluorescence spectroscopy and microscopy *J. Fluoresc.* **15** 377–413

[81] Höß P and Fleder K 2000 Time-integrated phosphor behavior in gated image intensifier tubes *Proc. SPIE* **4128** 23–8

[82] Höß P and Fleder K 2001 Response of very-fast-decay phosphors in image intensifier tubes for CCD readout devices *Proc. SPIE* **4183** 127–32

[83] Petrášek Z and Suhling K 2010 Photon arrival timing with sub-camera exposure time resolution in wide-field time-resolved photon counting imaging *Opt. Express* **18** 24888–901

[84] Hirvonen L M, Petrášek Z, Beeby A and Suhling K 2015 Microsecond wide-field TCSPC microscopy based on an ultra-fast CMOS camera *SPIE BiOS* **9329** 932939

[85] Dinu L, Eppink A T J B, Rosca-Pruna F, Offerhaus H L, van der Zande W J and Vrakking M J J 2002 Application of a time-resolved event counting technique in velocity map imaging *Rev. Sci. Instrum.* **73** 4206–13

[86] Strasser D, Urbain X, Pedersen H B, Altstein N, Heber O, Wester R, Bhushan K G and Zajfman D 2000 An innovative approach to multiparticle three-dimensional imaging *Rev. Sci. Instrum.* **71** 3092–8

[87] Hutchings J B, Postma J, Asquin D and Leahy D 2007 Photon event centroiding with UV photon-counting detectors *Publ. Astron. Soc. Pac.* **119** 1152–62

[88] Suhling K, Airey R W and Morgan B L 2002 Minimization of fixed pattern noise in photon event counting imaging *Rev. Sci. Instrum.* **73** 2917–22

[89] Suhling K, Airey R W and Morgan B L 1999 Optimisation of centroiding algorithms for photon event counting imaging *Nucl. Instrum. Methods Phys. Res.* A **437** 393–418

[90] Dick J, Jenkins C and Ziabicki J 1989 Design fundamentals of algorithms for photon-counting systems *Publ. Astron. Soc. Pac.* **101** 684–9

[91] Jenkins C R 1987 The image photon counting system: performance in detail, and the quest for high accuracy *Mon. Not. R. Astron. Soc.* **226** 341–60

[92] Bergamini P, Bonelli G, Paizis A, Tommasi L, Uslenghi M, Falomo R and Tondello G 2000 An imaging photon counting intensified CCD for high speed photometry *Exp. Astron.* **10** 457–71

[93] Bergamini P, Bonelli G, Tanzi E G, Uslenghi M, Poletto L and Tondello G 2000 A fast readout and processing electronics for photon counting intensified charge-coupled device *Rev. Sci. Instrum.* **71** 1841–8

[94] Uslenghi M, Fiorini M and Sarri G 2004 Wide dynamic range photon counting ICCD for ground-based astronomy *Nucl. Instrum. Methods Phys. Res.* A **518** 223–5

[95] Boksenberg A, Coleman C I, Fordham J and Shortridge K 1985 Interpolative centroiding in CCD-based image photon counting detectors *Adv. Electron. Electron Phys.* **64A** 33–47

[96] Bellis J G, Bone D A and Fordham J L A 1991 A new real-time centroiding technique for photon-counting detectors *Publ. Astron. Soc. Pac.* **103** 253–7

[97] Bulau S E 1986 Simulation of various centroiding algorithms *Proc. SPIE* **627** 680–7

[98] Carter M K and Read P D 1997 The implementation and performance of a connected regions centroiding algorithm for imaging photon counting *Nucl. Instrum. Methods Phys. Res.* A **392** 380–3

[99] Kawakami H, Bone D, Fordham J and Michel R 1994 The effect of event shape on centroiding in photon counting detectors *Nucl. Instrum. Methods Phys. Res.* A **348** 707–12

[100] Srivastava M K, Prabhudesai S M and Tandon S N 2009 Studying the imaging characteristics of ultra violet imaging telescope (UVIT) through numerical simulations *Publ. Astron. Soc. Pac.* **121** 621–33

[101] Michel R, Fordham J and Kawakami H 1997 Fixed pattern noise in high-resolution, CCD readout photon-counting detectors *Mon. Not. R. Astron. Soc.* **292** 611–20

[102] Blazit A *et al* 2008 New generation photon-counting cameras: Algol and CPNG *Appl. Opt.* **47** 1141–51

[103] Vallerga J, Tremsin A, Raffanti R and Siegmund O 2011 Centroiding algorithms for high speed crossed-strip readout of microchannel plate detectors *Nucl. Instrum. Methods Phys. Res.* A **633** S255–8

[104] Tremsin A S, Vallerga J V, Siegmund O H W and Hull J S 2003 Centroiding algorithms and spatial resolution of photon counting detectors with cross-strip anodes *Proc. SPIE* **5164** 113–24

[105] Hirvonen L M, Kilfeather T and Suhling K 2015 Single-molecule localization software applied to photon counting imaging *Appl. Opt.* **54** 5074–82

[106] Hirvonen L M, Barber M J and Suhling K 2016 Photon counting imaging and centroiding with an EBCCD using single molecule localisation software *Nucl. Instrum. Methods Phys. Res.* A **820** 121–5

[107] Clampin M, Crocker J, Paresce F and Rafal M 1988 Optical Ranicon detectors for photon counting imaging. I *Rev. Sci. Instrum.* **59** 1269–89

[108] Vallerga J V and McPhate J B 2000 Optimization of the readout electronics for microchannel plate delay line anodes *Proc. SPIE* **4139** 34–42

[109] Becker W, Hirvonen L M, Milnes J S, Conneely T, Jagutzki O, Netz H, Smietana S and Suhling K 2016 A wide-field TCSPC FLIM system based on an MCP PMT with a delay-line anode *Rev. Sci. Instrum.* **87** 093710

[110] Siegmund O H W, Tremsin A S, Vallerga J V and Hull J 2001 Cross strip imaging anodes for microchannel plate detectors *IEEE Trans. Nucl. Sci.* **48** 430–4

[111] Vallerga J, Raffanti R, Cooney M, Cumming H, Varner G and Seljak A 2014 Cross strip anode readouts for large format photon counting microchannel plate detectors: developing flight qualified prototypes of the detector and electronics *Proc. SPIE* **9144** 91443J

[112] Tremsin A S, Siegmund O H W, Vallerga J V, Raffanti R, Weiss S and Michalet X 2009 High speed multichannel charge sensitive data acquisition system with self-triggered event timing *IEEE Trans. Nucl. Sci.* **56** 1148–52

[113] Siegmund O H W, Vallerga J V, Tremsin A S, Hull J, Mane A U, Elam J W and O'Mahony A 2014 Optical and UV sensing sealed tube microchannel plate imaging detectors with high time resolution *Proc. of the Advanced Maui Optical and Space Surveillance Technologies Conf.*

[114] Lampton M and Malina R F 1976 Quadrant anode image sensor *Rev. Sci. Instrum.* **47** 1360–2

[115] Prokazov Y, Turbin E, Vitali M, Herzog A, Michaelis B, Zuschratter W and Kemnitz K 2009 Reborn quadrant anode image sensor *Nucl. Instrum. Methods Phys. Res.* A **604** 221–3

[116] Kemnitz K, Pfeifer L, Paul R and Coppey-Moisan M 1997 Novel detectors for fluorescence lifetime imaging on the picosecond time scale *J. Fluoresc.* **7** 93–8

[117] Kemnitz K, Pfeifer L and Ainbund M R 1997 Detector for multichannel spectroscopy and fluorescence lifetime imaging on the picosecond timescale *Nucl. Instrum. Methods Phys. Res.* A **387** 86–7

[118] Martin C, Jelinsky P, Lampton M and Malina R F 1981 Wedge-and-strip anodes for centroid-finding position-sensitive photon and particle detectors *Rev. Sci. Instrum.* **52** 1067–74

[119] Siegmund O H W, Lampton M, Bixier J, Chakrabarti S, Vallerga J, Bowyer S and Malina R F 1986 Wedge and strip image readout systems for photon-counting detectors in space astronomy *J. Opt. Soc. Am.* A **3** 2139–45

[120] Lapington J S, Milnes J S, Page M, Ingle M B and Rees K 2000 Novel electronic readout systems for photon-counting imagers *Proc. SPIE* **4128** 120–8

[121] Jagutzki O, Lapington J S, Worth L B C, Spillman U, Mergel V and Schmidt-Böcking H 2002 Position sensitive anodes for MCP read-out using induced charge measurement *Nucl. Instrum. Methods Phys. Res.* A **477** 256–61

[122] Lapington J S 2004 A comparison of readout techniques for high-resolution imaging with microchannel plate detectors *Nucl. Instrum. Methods Phys. Res.* A **525** 361–5

[123] Jagutzki O *et al* 2001 Multiple hit read-out of a microchannel plate detector with a three-layer delay-line anode *IEEE Trans. Nuclear Sci.* **49** 2477–83

[124] Rinnenthal J L *et al* 2013 Parallelized TCSPC for dynamic intravital fluorescence lifetime imaging: quantifying neuronal dysfunction in neuroinflammation *PLoS One* **8** e60100

[125] McLoskey D, Birch D J S, Sanderson A, Suhling K, Welch E and Hicks P J 1996 Multiplexed single-photon counting. I. A time-correlated fluorescence lifetime camera *Rev. Sci. Instrum.* **67** 2228–37

[126] Lapington J S, Ashton T J R, Ross D and Conneely T 2012 Progress towards a 256 channel multi-anode microchannel plate photomultiplier system with picosecond timing *Nucl. Instrum. Methods Phys. Res.* A **695** 78–82

[127] Tremsin A S, Vallerga J V, McPhate J B, Siegmund O H W and Raffanti R 2013 High resolution photon counting with MCP-timepix quad parallel readout operating at >1 kHz frame rates *IEEE Trans. Nucl. Sci.* **60** 578–85

[128] Fisher-Levine M and Nomerotski A 2016 TimepixCam: a fast optical imager with time-stamping *J. Instrum.* **11** C03016

[129] Poikela T *et al* 2014 Timepix3: a 65k channel hybrid pixel readout chip with simultaneous ToA/ToT and sparse readout *J. Instrum.* **9** C05013

[130] Cova S 1981 Towards picosecond resolution with single-photon avalanche diodes *Rev. Sci. Instrum.* **52** 408–12

[131] McIntyre R J 1985 Recent developments in silicon avalanche photodiodes *Measurement* **3** 146–52

[132] Rochas A, Gani M, Furrer B, Besse P A, Popovic R S, Ribordy G and Gisin N 2003 Single photon detector fabricated in a complementary metal-oxide-semiconductor high-voltage technology *Rev. Sci. Instrum.* **74** 3263–70

[133] Charbon E, Fishburn M, Walker R, Henderson R and Niclass C 2003 SPAD-based sensors *TOF Range-Imaging Cameras* (Berlin: Springer) pp 11–38

[134] Esposito A 2012 Beyond range: innovating fluorescence microscopy *Remote Sens.* **4** 111–9

[135] Krstajić N, Poland S, Levitt J, Walker R, Erdogan A, Ameer-Beg S and Henderson R K 2015 0.5 billion events per second time correlated single photon counting using CMOS SPAD arrays *Opt. Lett.* **40** 4305–8

[136] Luca P, Dutton N, Krstajic N, Calder N, Holmes A, Grant L A and Henderson A R 2015 A 256 × 256 SPAD array with in-pixel time to amplitude conversion for fluorescence lifetime imaging microscopy *Int. Image Sensor Workshop (Vaals, Netherlands)*

[137] Niclass C, Soga M, Matsubara H, Kato S and Kagami M 2013 A 100 m-range 10-frame s^{-1} 340 × 96 pixel time-of-flight depth sensor in 0.18 μm CMOS *IEEE J. Solid-State Circuits* **48** 559–72

[138] Krstajić N, Levitt J, Poland S, Ameer-Beg S and Henderson R 2015 256 × 2 SPAD line sensor for time resolved fluorescence spectroscopy *Opt. Express* **23** 5653–69

[139] Cuccato A, Antonioli S, Crotti M, Labanca I, Gulinatti A, Rech I and Ghioni M 2013 Complete and compact 32-channel system for time-correlated single-photon counting measurements *IEEE Photonics J.* **5** 6801514

[140] Pavia J M, Wolf M and Charbon E 2014 Measurement and modeling of microlenses fabricated on single-photon avalanche diode arrays for fill factor recovery *Opt. Express* **22** 4202–13

[141] Intermite G, McCarthy A, Warburton R E, Ren X, Villa F, Lussana R, Waddie A J, Taghizadeh M R, Tosi A, Zappa F and Buller G S 2015 Fill-factor improvement of Si CMOS single-photon avalanche diode detector arrays by integration of diffractive microlens arrays *Opt. Express* **23** 33777–91

[142] Richardson J A, Grant L A and Henderson R K 2009 Low dark count single-photon avalanche diode structure compatible with standard nanometer scale CMOS technology *IEEE Photonics Technol. Lett.* **21** 1020–2

[143] Siegmund O H W *et al* 2004 The GALEX mission and detectors *Proc. SPIE* **5488** 13–24

[144] Antonioli S, Cuccato A, Miari L, Labanca I, Rech I and Ghioni M 2013 Ultra-compact 32-channel system for time-correlated single-photon counting measurements *Proc. SPIE* **8773** 87730D

[145] Bronzi D, Villa F, Tisa S, Tosi A and Zappa F 2016 SPAD figures of merit for photon-counting, photon-timing, and imaging applications: a review *IEEE Sensors J.* **16** 3–12

[146] Niclass C and Soga M 2010 A miniature actively recharged single-photon detector free of afterpulsing effects with 6 ns dead time in a 0.18 μm CMOS technology *IEEE Int. Electron Devices Meeting* pp 14.3:1–4

[147] Scarcella C, Tosi A, Villa F, Tisa S and Zappa F 2013 Low-noise low-jitter 32 pixels CMOS single-photon avalanche diodes array for single-photon counting from 300 nm to 900 nm *Rev. Sci. Instrum.* **84** 123112

[148] Richardson J A, Webster E A G, Grant L A and Henderson R K 2011 Scaleable single-photon avalanche diode structures in nanometer CMOS technology *IEEE Trans. Electron Devices* **58** 2028–35

[149] Webster E A G, Richardson J A, Grant L A, Renshaw D and Henderson R K 2012 A single-photon avalanche diode in 90 nm CMOS imaging technology with 44% photon detection efficiency at 690 nm *IEEE Electron Device Lett.* **33** 694–6

[150] Bronzi D, Villa F, Tisa S, Tosi A, Zappa F, Durini D, Weyers S and Brockherde W 2014 100 000 frames s^{-1} 64 × 32 single-photon detector array for 2D imaging and 3D ranging *IEEE J. Sel. Top. Quantum Electron.* **20** 354–63

[151] Eisenhauer F and Raab W 2015 Visible/infrared imaging spectroscopy and energy-resolving detectors *Annu. Rev. Astron. Astrophys.* **53** 155–97

[152] Toussaint J *et al* 2012 Superconducting single-photon counting system for optical experiments requiring time-resolution in the picosecond range *Rev. Sci. Instrum.* **83** 123103

[153] Stevens M J, Hadfield R H, Schwall R E, Nam S W, Mirin R P and Gupta J A 2006 Fast lifetime measurements of infrared emitters using a low-jitter superconducting single-photon detector *Appl. Phys. Lett.* **89** 031109

[154] Peacock A *et al* 1996 Single optical photon detection with a superconducting tunnel junction *Nature* **381** 135–7

[155] Fraser G W, Heslop-Harrison J S, Schwarzacher T, Holland A D, Verhoeve P and Peacock A 2003 Detection of multiple fluorescent labels using superconducting tunnel junction detectors *Rev. Sci. Instrum.* **74** 4140–4

[156] Fraser G W, Heslop-Harrison J S, Schwarzacher T, Verhoeve P, Peacock A and Smith S J 2006 Optical fluorescence of biological samples using STJs *Nucl. Instrum. Methods Phys. Res.* A **559** 782–4

[157] Martin D D E, Verhoeve P, Peacock A, van Dordrecht A, Verveer J and Hijmering R 2004 A 12 × 10 pixels superconducting tunnel junction array based spectro-photometer for optical astronomy *Nucl. Instrum. Methods Phys. Res.* A **520** 512–5

[158] Dauler E A *et al* 2006 1.25 Gbit s^{-1} photon-counting optical communications using a two-element superconducting nanowire single photon detector *Proc. SPIE* **6372** 637212

[159] Marsili F *et al* 2013 Detecting single infrared photons with 93% system efficiency *Nat. Photon.* **7** 210–4

[160] Natarajan C M, Tanner M G and Hadfield R H 2012 Superconducting nanowire single-photon detectors: physics and applications *Supercond. Sci. Technol.* **25** 063001

[161] Gemmell N R, McCarthy A, Liu B, Tanner M G, Dorenbos S D, Zwiller V, Patterson M S, Buller G S, Wilson B C and Hadfield R H 2013 Singlet oxygen luminescence detection with a fiber-coupled superconducting nanowire single-photon detector *Opt. Express* **21** 5005–13

[162] Divochiy A *et al* 2008 Superconducting nanowire photon-number-resolving detector at telecommunication wavelengths *Nat. Photon.* **2** 302–6

[163] Marsili F *et al* 2015 Large-area arrays of WSi superconducting nanowire single photon detectors *Frontiers in Optics (OSA)* (doi:10.1364/FIO.2015.FW6B.5)

[164] Wang X, Setru S U, Xie J, Mane A, Demarteau M and Wagner R 2014 Imaging of large-area microchannel plates using phosphor screens *J. Instrum.* **9** P11011

[165] Jose M, Nair D K, Reissner C, Hartig R and Zuschratter W 2007 Photophysics of Clomeleon by FLIM: discriminating excited state reactions along neuronal development *Biophys. J.* **92** 2237–54

[166] Emiliani V, Sanvitto D, Tramier M, Piolot T, Petrášek Z, Kemnitz K, Durieux C and Coppey-Moisan M 2003 Low-intensity two-dimensional imaging of fluorescence lifetimes in living cells *Appl. Phys. Lett.* **83** 2471–3

[167] Vitali M, Reis M, Friedrich T and Eckert H-J 2010 A wide-field multi-parameter FLIM and FRAP setup to investigate the fluorescence emission of individual living cyanobacteria *Proc. SPIE* **7376** 737610–6

[168] Vitali M, Picazo F, Prokazov Y, Duci A, Turbin E, Götze C, Llopis J, Hartig R, Visser A J and Zuschratter W 2011 Wide-field multi-parameter FLIM: long-term minimal invasive observation of proteins in living cells *PLoS One* **6** e15820

[169] Nair D K, Jose M, Kuner T, Zuschratter W and Hartig R 2006 FRET-FLIM at nanometer spectral resolution from living cells *Opt. Express* **14** 12217–29

[170] Petrášek Z, Eckert H-J and Kemnitz K 2009 Wide-field photon counting fluorescence lifetime imaging microscopy: application to photosynthesizing systems *Photosynth. Res.* **102** 157–68

[171] Michalet X, Colyer R, Antelman J, Siegmund O, Tremsin A, Vallerga J and Weiss S 2009 Single-quantum dot imaging with a photon counting camera *Curr. Pharm. Biotechnol.* **10** 543–57

[172] Giraud G *et al* 2009 Fluorescence lifetime imaging of quantum dot labeled DNA microarrays *Int. J. Mol. Sci.* **10** 1930–41

[173] Giraud G *et al* 2010 Fluorescence lifetime biosensing with DNA microarrays and a CMOS-SPAD imager *Biomed. Opt. Express* **1** 1302–8

[174] Hirvonen L M, Becker W, Milnes J, Conneely T, Smietana S, Le Marois A, Jagutzki O and Suhling K 2016 Picosecond wide-field time-correlated single photon counting fluorescence microscopy with a delay line anode detector *Appl. Phys. Lett.* **109** 071101

[175] Barroca T, Balaa K, Delahaye J, Lévêque-Fort S and Fort E 2011 Full-field supercritical angle fluorescence microscopy for live cell imaging *Opt. Lett.* **36** 3051–3

[176] Barroca T, Balaa K, Lévêque-Fort S and Fort E 2012 Full-field near-field optical microscope for cell imaging *Phys. Rev. Lett.* **108** 218101

[177] Greger K, Neetz M J, Reynaud E G and Stelzer E H K 2011 Three-dimensional fluorescence lifetime imaging with a single plane illumination microscope provides an improved signal to noise ratio *Opt. Express* **19** 20743–50

[178] Weber P, Schickinger S, Wagner M, Angres B, Bruns T and Schneckenburger H 2015 Monitoring of apoptosis in 3D cell cultures by FRET and light sheet fluorescence microscopy *Int. J. Mol. Sci.* **16** 5375–85

[179] Suhling K, Hirvonen L M, Becker W, Smietana S, Netz H, Milnes J, Conneely T, Le Marois A and Jagutzki O 2016 Wide-field TCSPC-based fluorescence lifetime imaging (FLIM) microscopy *Proc. SPIE* **9858** 98580J

[180] Baggaley E, Weinstein J A and Williams J A G 2012 Lighting the way to see inside the live cell with luminescent transition metal complexes *Coord. Chem. Rev.* **256** 1762–85

[181] Dmitriev R I and Papkovsky D B 2012 Optical probes and techniques for O_2 measurement in live cells and tissue *Cell Mol. Life Sci.* **69** 2025–39

[182] Hirvonen L M, Fruhwirth G O, Srikantha N, Barber M, Neffendorf J E, Suhling K and Jackson T L 2016 Hydrodynamic radii of ranibizumab, aflibercept and bevacizumab measured by time-resolved phosphorescence anisotropy *Pharm. Res.* **33** 2025–32

[183] Terpetschnig E, Szmacinski H, Malak H and Lakowicz J R 1995 Metal-ligand complexes as a new class of long-lived fluorophores for protein hydrodynamics *Biophys. J.* **68** 342–50

[184] Kavandi J, Callis J, Gouterman M, Khalil G, Wright D, Green E, Burns D and McLachlan B 1990 Luminescent barometry in wind tunnels *Rev. Sci. Instrum.* **61** 3340–7

[185] Allison S W and Gillies G T 1997 Remote thermometry with thermographic phosphors: instrumentation and applications *Rev. Sci. Instrum.* **68** 2615–50

[186] Hirvonen L M, Festy F and Suhling K 2014 Wide-field time-correlated single-photon counting (TCSPC) lifetime microscopy with microsecond time resolution *Opt. Lett.* **39** 5602–5

[187] Hirvonen L M, Petrášek Z and Suhling K 2014 Wide-field time-correlated single photon counting (TCSPC) microscopy with time resolution below the frame exposure time *Nucl. Instrum. Methods Phys. Res.* A **787** 1–5

[188] Hirvonen L M, Petrášek Z, Beeby A and Suhling K 2015 Sub-μs time resolution in wide-field time-correlated single photon counting microscopy obtained from the photon event phosphor decay *New J. Phys.* **17** 023032

[189] Hemmati H 2014 *Near-Earth Laser Communications* (Boca Raton, FL: CRC Press)

[190] Shaw M *et al* 2015 Arrays of WSi superconducting nanowire single photon detectors for deep space optical communications *CLEO (Optical Society of America) p* JTh2A.68

[191] Buller G S and Wallace A M 2007 Ranging and three-dimensional imaging using time-correlated single-photon counting and point-by-point acquisition *IEEE J. Sel. Top. Quantum Electron.* **13** 1006–15

[192] McCarthy A, Collins R J, Krichel N J, Fernández V, Wallace A M and Buller G S 2009 Long-range time-of-flight scanning sensor based on high-speed time-correlated single-photon counting *Appl. Opt.* **48** 6241–51

[193] Jungmann J H and Heeren R M A 2013 Detection systems for mass spectrometry imaging—a perspective on novel developments with a focus on active pixel detectors *Rapid Commun. Mass Spectrom.* **27** 1–23

[194] Richards P and Lees J 2002 Functional proteomics using microchannel plate detectors *Proteomics* **2** 256–61

[195] Tarhoni M H, Vigneswara V, Smith M, Anderson S, Wigmore P, Lees J E, Ray D E and Carter W G 2011 Detection, quantification, and microlocalisation of targets of pesticides using microchannel plate autoradiographic imagers *Molecules* **16** 8535–51

[196] Turgeman L and Fixler D 2013 Time-averaged fluorescence intensity analysis in fluorescence fluctuation polarization sensitive experiments *Biomed. Opt. Express* **4** 868–84